THEIA:

THEIA Collaboration[1]

[1] *Many and Varied*

EXECUTIVE SUMMARY

The development of new scintillators in combination with high-efficiency, fast photon detection opens up the possibility for discrimination of Cherenkov and scintillation signals in large-scale detectors, offering both high light yield and directional information even at low threshold. Such a detector, situated in a fully-equipped deep underground laboratory, and utilizing developments in computing and reconstruction techniques, could achieve unprecedented levels of background rejection, thus enabling a physics program that would span topics in nuclear, high-energy, and astrophysics.

The Theia experiment targets a broad physics program, including a next-generation neutrinoless double beta decay search capable of reaching into the normal hierarchy region of phase space, sensitivity to solar neutrinos, supernova neutrinos, nucleon decay searches, and measurement of the neutrino mass hierarchy and CP violating phase.

This paper describes the technical breakthroughs that have led to the development of this detector concept, and the potential impact of such a detector on the fields of particle and astrophysics.

CONTENTS

I. INTRODUCTION AND THEIA OVERVIEW - GDOG, BOB, JRK, MICHI

The THEIA detector [**?**] leverages a tried and tested methodology in combination with novel, cutting-edge technology. The future of neutrino detection technology lies in massive, high-precision detectors, offering multiple channels for detection. Current technology is constrained by the choice of target material: water detectors are limited in energy threshold and resolution by the overall light yield of the Cherenkov process, and scintillator detectors are limited in size by optical attenuation in the target itself, and in reconstruction of event direction by the isotropic nature of scintillation light.

The newly-developed water-based liquid scintillator (WbLS) [1] offers a unique combination of high light yield and low-threshold detection with attenuation close to that of pure water, particularly at wavelengths > 400 nm. Use of this novel target material could allow separation of prompt, directional Cherenkov light from the more abundant, isotropic, delayed scintillation light. This would be a huge leap forwards in neutrino detection technology, enabling the first low-threshold, directional neutrino detector. Such a detector could achieve fantastic background rejection using directionality, event topology, and particle ID. WbLS chemistry also allows loading of metallic ions as an additional target for particle detection, including: ^{7}Li for charged-current solar neutrino detection; $^{\mathrm{nat}}$Gd for neutron tagging enhancement; or isotopes that undergo double beta decay, facilitating a neutrinoless double-beta decay (NLDBD) program. The formula and principle of mass-produced WbLS have been developed and demonstrated at the Brookhaven National Laboratory Liquid Scintillator Development Facility. Metal-doped samples have been produced with high stability, with loadings of up to several percent. The instrumentation for large-scale liquid production is currently under design.

THEIA would combine the use of a 30–100-kton WbLS target, doping with a number of potential isotopes, high efficiency and ultra-fast timing photosensors, and a deep underground location. A potential site is the Long Baseline Neutrino Facility (LBNF) far site, where THEIA could operate in conjunction with the liquid argon tracking detector proposed by DUNE [**?**]. The basic elements of this detector are being developed now in experiments such as WATCHMAN [**?**], ANNIE [**?**] and SNO+ [**?**].

A large-scale WbLS detector such as THEIA can achieve an impressively broad program of physics topics, with enhanced sensitivity beyond that of previous detectors. Much of the program hinges on the capability to separate prompt Cherenkov light from delayed scintillation. This separation provides many key benefits, including:

- The ring-imaging capability of a pure water Cherenkov detector (WCD). This enables a long-baseline program in a scintillation-based detector, with the additional benefit of low-threshold

detection of hadronic events.

- Direction reconstruction using prompt Cherenkov photons. This allows statistical identification of events such as solar neutrinos, which offer a rich physics program in their own right, as well as forming a background to many rare-event searches, including NLDBD and nucleon decay.
- Low thresholds and good energy and vertex resolution using the abundant scintillation light.
- Detection of sub-Cherenkov threshold scintillation light. This provides excellent particle identification, including enhanced neutron tagging, detection of sub-Cherenkov threshold particles such as kaons in nucleon decay searches, and separation of atmospheric neutrino-induced neutral current backgrounds for inverse beta decay searches.

One of the most powerful aspects of THEIA is the flexibility: in the target medium itself, and even in the detector configuration. The WbLS target can be tuned to meet the most critical physics goals at the time by modifying features of the target cocktail, including: the fraction of water vs scintillator; the choice of wavelength shifters and secondary fluors; and the choice of loaded isotope. There is also the potential to construct a bag to contain isotope, and perhaps a higher scintillator-fraction target, in the centre of the detector, building on work by KamLAND-Zen [**?**] and Borexino [**?**].

A. Detector configuration

Include TWO baseline designs – ideal and "realistic" (existing cavern)
Include description of phased deployment e.g. refer to THEIA-i, THEIA-ii, THEIA-iii
Define the baseline design for each here, so that physics sections can simply refer back
e.g. THEIA-ii might be 50ktonne 10% WbLS, 90% coverage
whereas THEIA-iii might be the above with 5% WbLS but a bag containing LS + Te/Xe

II. TECHNOLOGY DEVELOPMENTS

A. Water-based Liquid Scintillator - R. Svoboda

There are a number of demonstrations required in order to realize the conceptual detector presented here. These include (but are not limited to):

1. Sufficiently high intrinsic light yield and long attenuation length to meet minimal light collection requirements. (This requirement can be offset by high efficiency, high coverage photon detection).

2. Successful separation of Cherenkov and scintillation signals, with sufficiently high Cherenkov light yield to maintain direction resolution and ring imaging capability. This can be achieved by ultra-fast timing photon detection, such as LAPPDs, tuning of the WbLS cocktail, or a combination of the two.

3. Stability of the above properties over long timescales, and with respect to isotope loading (*e.g.* Gd, Li, Te).

4. Materials compatibility studies.

5. Demonstrated reconstruction & particle ID capability.

The R&D program for THEIA strongly leverages existing efforts and synergy with other programs, such as WATCHMAN [**?**], ANNIE [**?**], SNO+ [**?**] and others. Ongoing work includes WbLS development at BNL, purification and compatibility studies at UC Davis, characterization and optimization with the CHESS detector at UC Berkeley and LBNL [**? ?**], fast photon sensor development at ANL, U Chicago, Iowa State and others [**?**], development of reconstruction algorithms [**? ?**], and potential nanoparticle loading in NuDot at MIT [**?**].

B. Photon Sensors - volunteers?

C. Reconstruction Techniques – B. Wonsak & M. Tsanov

While in the past Cherenkov detectors have been very successful in reconstructing various properties of the particles involved in a neutrino event, liquid scintillation detectors have long been thought as a source for calorimetric information only. However, in recent years it became obvious that the time information of the light in liquid scintillators can be used to access a wide range of information, similar or even superior to what a pure Cherenkov detector can deliver.

Basically, there are two complementary approaches to reconstruction in both detector types and consequently also in WBLS detectors. The first approach developed in MiniBooNE[**?**] and successfully applied in T2K[**?**] follows a likelihood ansatz to find the optimal track parameters and compare different hypotheses. In contrast to this, the three-dimensional topological reconstruction tries to picture the spatial distribution of the energy deposition within the detector without using a specific hypothesis. This technique has been developed for the LENA[**?**] detector and also been implemented for the JUNO detector [**?**]. These are liquid scintillator detectors, but the application to Cherenkov detectors is straight forward.

Both methods have been improved considerably over the last couple of years. For example fitQun, the reconstruction software used by T2K is now able to reconstruct up to 6 Cherenkov rings. This alone will increase the expected sensitivity for example for CP-violation in the LBNF beam significantly in comparison to previous studies like [**?**]. In addition, the topological reconstruction promises large volume liquid detectors the same capabilities as only highly segmented detectors used to have (with all the implications of that). This includes possibilities for particle identification at energies as low as a few MeV based on topological information. This ability will be further enhanced by the combination of the two light species, Cherenkov and scintillation light, as can be seen in [**?**], where Cherenkov-Scintillation separation is used to identify the two electrons of a $0\nu\beta\beta$-decay.

To give an overview on the state of the art in reconstruction, this section is divided into three subsections. The first subsection is dedicated to the likelihood approach and its latest results. The second subsection describes the topological reconstruction. And the third subsection is dedicated to applications of Cherenkov-light-Separation at low energies.

1. Likelihood

This subsection summarizes the main features of the reconstruction method developed for the MiniBooNE detector[**?**]. In this method a likelihood function is evaluated for a particle (particles) of some type with initial kintmatic parameters to have produced the observed collection of PMT hits, charges and times, in an event. A key ingredient of the likelihood calculation is the predicted hit

distribution which represents the average response of the detector for such a particle and therefore the likelihood is a function of the paricle's kinematic parameters. The optimal parameters would provide the best agreement between the predicted and observed hit distributions i.e. the likelihood function will be at a maximum.

Realistic model of detector response is required to develop a successful and efficient event reconstruction and identification algorithms. This requires both *in-situ* and *ex-situ* measurements of various optical properties of the water, PMTs and the reflection of all surface inside the detector. Absorption, scattering, reflections and fluorescence processes can affect the reconstruction. In order to account for these effects in the reconstruction, these optical properties have to be obtained if unknown.

Single track is parametrized with 7 parameters: starting point (x_0, y_0, z_0), starting time t_0, direction θ_0, ϕ_0 with respect to the beam and kinetic energy E_0. We refer to this vector as $\mathbf{u}$. Track information is obtained by maximizing the likelihood that track with vector $\mathbf{u}$ will produce the observed PMT measurements. The likelihood for an event assuming all PMTs are independent is given by

$$L(\mathbf{q}, \mathbf{t}; \mathbf{u}) = \prod_{i}^{N_{unhit}} P_i(\text{unhit}; \mathbf{u}) \times \prod_{j}^{N_{hit}} P_j(\text{hit}; \mathbf{u}) f_q(q_j; \mathbf{u}) f_t(t_j; \mathbf{u}). \tag{1}$$

Here $P_i(\text{unhit}; \mathbf{u})$ is the probability PMT i is not hit given $\mathbf{u}$, $P_i(\text{hit}; \mathbf{u})$ is the probability PMT i is hit given $\mathbf{u}$, $f_q(q_j; \mathbf{u})$ is the probability density function for the measured charge q given $\mathbf{u}$ and predicted charge q_j, $f_t(t_j; \mathbf{u})$ is the probability density function for the measured time t given $\mathbf{u}$ evaluated time t_j. Product is carried over all PMTs. For convenience we can work with the negative logarithm of the likelihood which can be written as a sum of negative logarithms. We will use F_q and F_t to denote the charge and the time negative logarithm likelihoods respectively

$$-\log L(\mathbf{u}) \equiv F_q(\mathbf{u}) + F_t(\mathbf{u}), \tag{2}$$

$$F_t(\mathbf{u}) = -\sum_{i}^{N_{hit}} \log f_t(t_i; \mathbf{u}), \tag{3}$$

$$F_q(\mathbf{u}) = -\sum_{i}^{N_{unhit}} \log P_i(\text{unhit}; \mathbf{u}) - \sum_{i}^{N_{hit}} \log P_i(\text{hit}; \mathbf{u}) - \sum_{i}^{N_{hit}} \log f_q(q_i; \mathbf{u}). \tag{4}$$

From here on we will refer to F_q and F_t simply as the charge and the time likelihoods.

If the number of observed photoelectrons (PE), n_i, is known for a given PMT one can assume that $f_q(q_i;\mathbf{u})$ is fully specified regardless of detector properties. In addition, n_i can be assumed to be Poisson distributed with a mean value $\mu_i(\mathbf{u})$ (predicted charge) for which the notation μ_i will be used with implicit dependence on $\mathbf{u}$. As a result, the probability for a PMT to have no hit is

$$P_i(\text{unhit};\mathbf{u}) \equiv \overline{P}_i(\mu_i) = e^{-\mu_i}. \tag{5}$$

Hence, the probability a PMT has recorded a hit is

$$P_i(\text{hit};\mathbf{u}) \equiv P_i(\mu_i) = 1 - \overline{P}_i(\mu_i). \tag{6}$$

The next step is to separate the predicted charge into prompt and late predicted charge

$$\mu_i \equiv \mu_{prompt,i} + \mu_{late,i}. \tag{7}$$

The prompt predicted charge is a result of Čerenkov light, while the late predicted charge has contributions from direct Čerenkov light and indirect light. Sources of indirect light are reflections, scattering and fluorescence.

Time PDFs $f_t(t_i;\mathbf{u})$ depend on the first photon to fire the PMT. Dependence on $\mathbf{u}$ can be reduced by introducing corrected time

$$t_{cor,i} = t_i - t_0 - \frac{r_{mid,i}(E_0)}{c_n} - \frac{\Delta s_{mid}(E_0)}{c}, \tag{8}$$

where t_i is the measured PMT time, t_0 is the measured start time, $\Delta s_{mid}(E_0)$ is the distance from the track start point to the mean Čerenkov emission point, $r_{mid,i}(E_0)$ is the distance from the mean Čerenkov emission point to the PMT, c_n and c are the speeds of light in water and vacuum respectively. Due to the latency period PMT can register only one hit for a given track. Probabilities of no prompt PEs and no late PEs can be written as $P(\text{no prompt PEs}) = e^{-\mu_{prompt}}$ and $P(\text{no late PEs}) = e^{-\mu_{late}}$ respectively. The probability that a hit contains at least one prompt PE is

$$w_p = P(\text{prompt PE present}|hit) = \frac{1 - P(\text{no prompt PEs})}{1 - P(\text{no prompt PEs})P(\text{no late PEs})}. \tag{9}$$

This is the weight for the prompt primitive distribution $G_{ch}(t_c, E_0, \mu_{prompt})$, while the $w_l = 1 - w_p$ is the weight for the late primitive distribution $G_{late}(t_c, E_0, \mu_{late})$. Finally, the time PDF is obtained

from

$$f_t(t; E_0, \mu_{prompt}, \mu_{late}) = w_p G_{ch}(t_c, E_0, \mu_{prompt}) + w_l G_{late}(t_c, E_0, \mu_{late}). \tag{10}$$

The primitives distribution are created by generating particles throughout the detector in special runs (e.g. only Čerenkov light and no scattering) and the response is parametrized.

2. 3D topological reconstruction

In this subsection a reconstruction method is presented which aims to provide a 3D topological representation of the energy deposition of an event. The method has already been described in detail in [**?**]. Thus, here only a short description of the basic concepts is given.

a. Basic idea The general idea of this method is to use the timing information of all registered signals for the construction of isochronal surfaces around each light sensor defined by the signal time. The overlap of these surfaces then indicates likely points of origin of the detected photons and thus can reflect the spatial distribution of the energy deposition of an event. The only assumptions made within this method are that a reference point on the topology is known reasonably well in space and time (the time of the energy deposition) and that all particles propagate through this point in approximately straight lines with the speed of light. The necessary reference point has to be provided by a prior analysis of the event. For the sake of simplicity we assume in the following that it is the primary vertex of the event. The isochrones can then be described by

$$c \cdot t_{signal} = |\overline{VX}| + n \cdot |\overline{XP}| \,, \tag{11}$$

where n is the effective refraction index for the scintillation light, $|\overline{VX}|$ is the distance between the vertex V of the event and the point of photon emission X, while $|\overline{XP}|$ is the distance between the point X and the PMT P.

These isochrones need to be smeared out using a time profile $F(t)$ given by the scintillator properties as well as the time resolution of the optical sensors used. This results in a probability density distribution for each signal. Furthermore, the position dependend light detection efficiencies of the PMT have to be taken into account as well as detector effects leading to different light emission in different regions (e.g. a buffer region). We combine these light distribution effects in the function $LD(\vec{x})$.

The full topological image of the event is then generated by adding up the individual probability density distribution $P_i(\vec{x})$:

$$P(\vec{x})_{total} = \sum_i P_i(\vec{x}) = \sum_i \left[\frac{F_i(t(\vec{x})) \cdot LD_i(\vec{x})}{\iiint F_i(t(\vec{x})) \cdot LD_i(\vec{x}) \cdot d\vec{x}} \right] . \tag{12}$$

Here, the index i indicates the individual signals. Thus the $F_i(t(\vec{x}))$ have to be evaluated with the individual signal times $t_{signal,i}$ and the position P_i of the PMT which detected the signal (see equation 13), while LD_i is an attribute of this PMT depending on its position, optics and sensitivity.

$$F_i(t(\vec{x})) = F_i\left((|\overline{VX}| + n \cdot |\overline{XP}|_i)/c \right) . \tag{13}$$

The result is a 3d map of the expected mean number of detected photons $\langle N_D(\vec{x}) \rangle$ coming from a given point. However, to get an impression of the energy deposition for a given event, the number of photons emitted from that point $\langle N_E(\vec{x}) \rangle$ is deciding. Therefore, every point of the 3d distribution has to be weighted by the inverse of the total signal detection efficiency $\eta(\vec{x})$ at that point:

$$\langle N_E(\vec{x}) \rangle = \frac{\langle N_D(\vec{x}) \rangle}{\eta(\vec{x})} = \frac{P(\vec{x})_{total}}{\sum_{PMT} LD_{PMT}(\vec{x})} \tag{14}$$

In principle, the reconstruction is completed at this stage. However, due to the large width of the time distribution of the individual signals, the picture may not seem very sharp. On the other hand, the large number of photons involved still generates a very good spatial resolution of the event topology. To extract this information, further algorithms are neccessary. For this purpose, standard algorithms developed originally for 2D image processing - like filtering, ridge-line finding, Sobel filter, etc. - can be adapted to accommodate 3D data.

b. Iteration procedure In the method above all signals have been treated as completly independend of each other. However, this is not true because all of them belong to the same event and the resulting correlation can be described by the true event toplogy. This topology is of course unknown. However, if we dispose of a certain prior knowledge about that topology, we can express this as a 3D probability density distribution $PM(\vec{x})$. Instead of calculating our topological 3D-picture from the completely independent 3D probability density distributions $P(\vec{x})_i$, we can now calculate this topology under the condition that it has to match our knowledge $P(\vec{x}|PM(\vec{x}))_i$. In other words, if we already

have a 3d representation of the event, which we call in this context probability mask (PM), we can use this to reweight the 3D probability density distribution generated by every single photon prior to its normalisation: Thus the $P_i(\vec{x})$ in Equation 12 have to be substituted by

$$P_i(\vec{x}|PM(\vec{x})) = \frac{F_i(t(\vec{x})) \cdot LD_i(\vec{x}) \cdot PM(\vec{x})}{\iiint F_i(t(\vec{x})) \cdot LD_i(\vec{x}) \cdot PM(\vec{x}) \cdot dV} \tag{15}$$

A natural choice to generate a PM, is to use the reconstruction as described on the previous pages first without a PM. The result of this reconstruction then constitutes an unbiased representation of the event topology, which can then be used as the PM for a second iteration of the reconstruction. The result of this second reconstruction can again be fed back as a new PM into the reconstruction process. Thus an iterative procedure is created. The power of this iterative process can be seen in Fig. 1. Ultimately, this allows a close association of each signal photon with a certain volume of the event topology. This makes the energy deposition per unit length accessible as can bee seen in Fig. 1.

c. Results So far this method has mainly been studied with the help of the LENA simulation. This simulation includes only an effective optical model and no Cherenkov light. Furthermore, it was assumed that every photon could be registered separatly. LENA has a coverage of 30% resulting in approximatly 250 detected photons per MeV. To reduce the computation time for the reconstruction an adaptive mesh was used. This allowed to establish a voxel size of 12.5 cm in the final iteration. More details about the simulation and the technical implementation of the topological reconstruction can be found in [**?**].

To proof the robustness and show the potential of this method a large sample of fully contained muons with energies between 1 and 10 GeV was used. An angular resolution between 1.4° at 1 GeV and 0.4° at 10 GeV could be achieved. In addition, the method has been implemented for the JUNO [**?**] detector. First results indicate a high potential for the separation of perfectly point-like events (electrons) from almost point-like events (positrons and gammas) at energies of a few MeV (compare [**?**]).

d. Application to Cherenkov light Some modifications are needed for the application of this method to Cherenkov light. The most obvious one is the time profile $F(t)$, since the Cherenkov process emits the light instantaneously. Thus in most scenarios the timing profile of the photosensors will be the dominant factor, which can often be described by a Gaussian with the corresponding time resolution. However, chromatic dispersion of the Cherenkov light must be taken into account if sensors with very good time resolution (below 1 ns) are employed in detectors of the size of THEIA.

In addition the position dependent detection efficiencies also become direction dependent now, since the Cherenkov light is emitted only in a cone with respect to the particle direction. How to generate such direction dependent detection efficiencies is shown for example in [**?**]. However, in general they differ for different particles due to the different behaviour when passing through matter. To avoid this, we start instead with the basic method without any light distribution effect (detection efficiencies). Thanks to the good timing quality of the Cherenkov-light this already allows to define an accurate volume of interest. In principle, this toplogy can then be used for the descion on the direction dependent detection efficiencies. However, this still has to be demonstrated.

3. Low-energy reconstruction

by Andrey

III. PHYSICS SENSITIVITIES AND DETECTOR REQUIREMENTS

THEIA would address a broad program of physics, including: geo-neutrinos, supernova neutrinos, nucleon decay, measurement of the neutrino mass hierarchy and CP violating phase, and even a next-generation NLDBD search.

A. Long Baseline - M Wilking for LBL group

B. Nucleon Decay - volunteers?

a. Motivation BRIEF intro to physics motivation, and status of the field: our major competitors

b. XX with THEIA What we bring to the table - pros of THEIA design

Sensitivity estimates with baseline design (one of THEIA i–iii)

c. Detector Requirements A summary of the impact of different detector choices i.e. what happens if we stray from the relevant baseline

C. Atmospheric Neutrinos - volunteers?

a. Motivation BRIEF intro to physics motivation, and status of the field: our major competitors

b. XX with THEIA What we bring to the table - pros of THEIA design

Sensitivity estimates with baseline design (one of THEIA i–iii)

c. Detector Requirements A summary of the impact of different detector choices i.e. what happens if we stray from the relevant baseline

D. Neutrinoless Double Beta Decay - L Winslow, V Lozza, A Mastbaum for DBD group

The THEIA search for neutrinoless double beta decay (NLDBD) aims for sensitivity to the non-degenerate normal hierarchy parameter space within the canonical framework of light Majorana neutrino exchange and three-neutrino mixing, at the level of $m_{\beta\beta} \sim 5$ meV. This is achieved through the loading of a very large mass of a NLDBD candidate isotope into an ultra-pure liquid scintillator target, together with coincidence and topological particle identification techniques.

1. Detector Configuration

a. Target Medium For the present studies, we consider a target that consists of pure LAB liquid scintillator loaded with the NLDBD isotope. This volume is contained within a nylon balloon, and the region of the detector outside is filled with water-based liquid scintillator (WbLS) with no isotope loading. With loading at 3% by mass, a 25 ton (55 ton) experiment corresponds to a 6.4 m (8 m) radius containment balloon.

b. Isotope Loading We consider possible NLDBD searches using two candidate isotopes: Te and Xe. In the case of Xe loading, xenon gas 89.5% enriched in ^{136}Xe is dissolved directly into the liquid scintillator, while Te loading is achieved via a novel technique developed for the SNO+ experiment and uses natural Te (34.1% ^{130}Te). The contamination associated with the materials used for Te loading are considered in the background assessment.

Additional NLDBD isotopes may be considered as long as they can be loaded into liquid scintillator. A staged approach is envisioned where an NLDBD observation in one isotope can be confirmed by removing it and deploying a second; the ability to switch isotopes is a key advantage of a liquid scintillator detector.

2. Backgrounds

The main sources of background near the NLDBD energy region of interest include:

Double Beta Decay: This irreducible background is due to the $2\nu\beta\beta$ decays of ^{130}Te or ^{136}Xe. Due to the steeply-falling spectrum, the number of events falling in the ROI depends strongly on the

energy resolution.

Cosmogenic Production: These backgrounds are due to activation of nuclei by muons (during data taking) or protons and neutrons (during material production and handling at Earth's surface).

Solar Neutrinos: The primary source is elastic scattering of ^{8}B solar neutrinos, though these events can potentially be reduced using the direction relative to the Sun. Another potential background is due to activation of the target material (Te or Xe) by the solar neutrinos, mainly ^{7}Be and ^{8}B neutrinos; this background is also dependent on the energy resolution.

Internal Contamination: Decays from U- and Th-chain impurities present in the scintillator mixture. Due to the large Q value of the candidate NLDBD isotopes, the two important backgrounds are due to ^{214}Bi (Q = 3.27 MeV) and ^{208}Tl (Q = 5 MeV). The scintillator purity can be improved by purification techniques to levels better than 10^{-18}, as demonstrated by the Borexino experiment [2].

External Sources: Decays from U and Th-chain impurities present in the balloon material, the external water-based liquid scintillator, the shielding water, and in the PMTs also contribute to the background. The two most important isotopes are ^{214}Bi and ^{208}Tl, as they decay by the emission of high energy ($E > 2$ MeV) γ rays that can travel long distances. These events can be reduced using a fiducial volume cut, though the balloon material remains the most important as it is closest to the target volume.

A summary of all the expected background events is given in Table I.

a. Cosmogenic Backgrounds The cosmogenically-induced background consists of nuclides produced by activation of the target material by neutrons, protons, and muons during production, handling, storage, and data-taking.

Long-lived, high Q value nuclides can be produced by neutron and proton activation mainly while the material is on the Earth's surface. The production in Xe and Te has been investigated by several authors [3–9]. Among the most important nuclides are ^{60}Co (Q = 2.8 MeV, $T_{1/2}$ = 5.27 y) and ^{110m}Ag (Q = 3.1 MeV, $T_{1/2}$ = 250 d). Mitigation of these background sources requires minimal exposure at sea level, a deep underground cool-down period, and chemical purification processes [10].

Neutron activation can also happen deep underground, while the experiment is running. Neutrons originate from the radioactivity and from muon-induced reactions in the rock. A water shield will provide a mitigation, as the majority of the neutrons will thermalize and stop before reaching the target material.

Source	Target level	Expected events/y $r = 6.4$ m	Expected events/y $r = 8$ m
Balloon ^{10}C		250 – 800	500 – 1600
^{8}B neutrinos		1522	2950
^{130}I (Te target)		80 (15 from ^{8}B)	155 (30 from ^{8}B)
^{136}Cs (Xe target)		24 (3 from ^{8}B)	47 (6 from ^{8}B)
^{136}Cs ($^{\text{enr}}$Xe target)		245 (35 from ^{8}B)	478 (68 from ^{8}B)
$2\nu\beta\beta$ (Te target)		6.3×10^{7}	1.2×10^{8}
$2\nu\beta\beta$ (Xe target)		3.6×10^{6}	7.0×10^{6}
$2\nu\beta\beta$ ($^{\text{enr}}$Xe target)		3.6×10^{7}	7.1×10^{7}
Liquid scintillator	^{214}Bi: 10^{-17} g_U/g	3700	7300
	^{208}Tl: 10^{-17} g_{Th}/g	440	870
Nylon Vessel	^{214}Bi: $< 1.1 \times 10^{-12}$ g_U/g	7.7×10^{4}	1.2×10^{5}
	^{208}Tl: $< 1.6 \times 10^{-12}$ g_{Th}/g	1.3×10^{4}	2.1×10^{4}
PMTs	^{214}Bi: 10^{-6} g_U/PMT		
	^{208}Tl: 10^{-6} g_{Th}/PMT		

TABLE I: Dominant background sources expected for the NLDBD search in THEIA. It is assumed that the Te or Xe isotopes are directly loaded at a level of 3%(Xe) or 5% (Te) in the LAB+PPO scintillator cocktail. The total mass is 28.3 tonnes (6.4 m radius) or 55 tonnes (8 m radius) for the 3% loading and 47 tonnes (6.4 m radius) or 92.5 tonnes (8 m radius) for the 5% loading.

For the purpose of this paper, it is assumed that the material will have a minimum exposure time at sea level and will be stored underground long enough to allow all the potential cosmogenic-induced nuclides produced during the surface exposure to decay.

A different source of cosmogenic background is the muon activation of the material during the data-taking period. In particular a potential background is the production of ^{10}C ($Q = 3.65$ MeV, $T_{1/2} = 19.3$ s) by muon interaction with the carbon atoms of the liquid scintillator. The interaction is accompanied by the emission of two neutrons. ^{10}C decays via the emission of a positron of 1.87 MeV end-point energy, followed by the emission of a γ of 0.72 MeV total energy. A mitigation strategy for this background source consists of a three-fold coincidence technique as developed by Borexino and KamLAND [11, 12], making use of the muon trajectory, the 2.2 MeV γ emitted by the neutron capture, and the ^{10}C decay. Additionally, the γ may travel away from the positron stopping point several tens of centimeters. This event topology is different from the neutrinoless double-beta decay, in which the energy deposition is localized.

The event rate of muon induced ^{10}C decays can be estimated following Reference [13]. The muon flux expected at the Homestake 4850 level (4300 mwe) is 4.2×10^{-9} cm^{-2} s^{-1}, while the calculated average muon energy at the same depth is 293 GeV [14]. The LAB+PPO mixture has a ^{12}C density

of 4.4×10^{31} atoms/kt. The following formula can be used to scale the density from the one measured in Borexino and KamLAND:

$$R_i = R_{data} \times \left(\frac{\langle E_\mu \rangle}{\langle E_{\mu,data} \rangle} \right)^{\alpha_{sim}} \times \frac{\Phi_\mu}{\Phi_{\mu,data}} \times \frac{n_{12C}}{n_{12C,data}} \tag{16}$$

where α_{sim} has been obtained from FLUKA/Geant4 simulation and is equal to 0.7621 for ^{10}C [15]. This results in about 300 events/kt/yr. Using Equation 10 in Reference [13] results in about 800 events/kt/yr. For this source of background a reduction of 92.5% is assumed based on what reached by Borexino [16]

b. Solar Neutrino Induced Background ^{8}B solar neutrino elastic scattering in the target material results in a background that is approximately flat across the NLDBD energy region of interest. The spectrum can be normalized using the total ^{8}B flux and best fit solar mixing parameters, as in Reference [17]. The expected rate is about 1600 events/yr/kt of target material.

Another source of background are the nuclides produced by charged current interaction of solar neutrinos with Te or Xe, in particular ^{130}Te and ^{136}Xe. A detailed study of the expected interaction rate is given in References [25, 26].

For ^{130}Te (34.08% natural abundance) a total of 33.7 SNU are expected, of which 6.1 SNU due to ^{8}B neutrinos and 20.9 SNU due to ^{7}Be neutrinos. The daughter isotope is ^{130}I in the 1^+ excited state. The excited states decay quickly to the first excited level, which decays with $T_{1/2} = 8.84$ min to the ground state via internal transition (branching ratio 84%, $E_\gamma = 40$ keV), or directly beta decays to ^{130}Xe with a Q value of 2.99 MeV (BR = 16%). The ground state beta decays with a Q value of 2.95 MeV and a $T_{1/2} = 12.4$ h. Due to the long half life a tagging technique based on a delayed coincidence might have a small efficiency.

For ^{136}Xe (8.8573% natural abundance) a total of 68.8 SNU are expected, of which 9.8 SNU due to ^{8}B neutrinos and 46 SNU due to ^{7}Be neutrinos. The resulting isotope is ^{136}Cs in the 1^+ excited states. The excited states decay quickly to the ground state, which decays with $T_{1/2} = 13.16$ d via beta decay (branching ratio = 100%) with a Q value of 2.55 MeV. Again in this case, a tagging technique based on a delayed coincidence will have only a small effect on removing this source of background due to the long half life.

The expected rate of events is given in Table I.

c. Double Beta Decay Backgrounds The number of $2\nu\beta\beta$ decays for ^{130}Te is calculated using the half life measured by CUORE [18], $T_{1/2} = (8.2 \pm 0.2\ (\text{stat.}) \pm 0.6\ (\text{syst.})) \times 10^{20}$ y. This results in a

rate of events per year

$$R_{2\nu\beta\beta} = 1.33 \times 10^7 \times M \times f \tag{17}$$

where M is the mass inside the balloon in kt and f is the loading fraction of natural isotope, or 1.2×10^8 events/yr for the 5% loading and a 8 m radius balloon.

For ^{136}Xe, the half life measurement in [12, 19] is used, $T_{1/2} = (2.165 \pm 0.016\ (\text{stat.}) \pm 0.059\ (\text{syst.})) \times 10^{21}$ y, for a rate of

$$R_{2\nu\beta\beta} = 1.26 \times 10^6 \times M \times f \tag{18}$$

or 7.0×10^6 events/y for the 3% loading and a 8 m radius balloon. In case a 89.5% enriched ^{136}Xe is used, the expected number of events is 7.1×10^7 events/yr within a 8 m radius balloon.

d. Scintillator Backgrounds A high purity level required in the LAB+PPO cocktail used to fill the balloon can be obtained using various purification techniques, including liquid-liquid extraction, nano-filtration, steam stripping, and distillation. A level of 10^{-17} g/g in both U and Th has been demonstrated by the KamLAND [20] and the Borexino [21] experiments. More recently a purity level of better than 10^{-18} has been obtained for the Phase-II of Borexino [2]:

^{238}U: $< 9.7 \times 10^{-19}$ g/g (95% CL from ^{214}Bi-Po)

^{232}Th: $< 1.2 \times 10^{-18}$ g/g (95% CL from ^{212}Bi-Po)

In addition to chemical purification, delayed coincidence techniques can be used to reduce the number of ^{214}Bi decays falling in the ROI. ^{214}Bi ($T_{1/2} = 19.9$ min) beta decays to ^{214}Po with a Q value of 3.27 MeV in 99.979% of cases. Several experiments have shown that this decay can be tagged using the subsequent ^{214}Po alpha-decay ($T_{1/2} = 164.3\,\mu$s, $E_\alpha = 7.7$ MeV). A rejection >99.95% for the ^{214}BiPo events falling in the region of interest has been demonstrated by the KamLAND-Zen experiment [30]. Monte Carlo studies for the SNO+ experiment show that the rejection in the double-beta decay region can be improved, reaching nearly 99.99%, by combining delayed coincidences cuts and PMT time information of the events [10].

In the remaining 0.021% of the cases ^{214}Bi alpha-decays to ^{210}Tl ($T_{1/2} = 1.3$ min), which beta decays to ^{210}Pb with a Q value of 5.5 MeV. An α–β delayed coincidence, can be applied in this case. However, due to the longer half-life of ^{210}Tl, the tagging technique is expected to be less efficient.

In the case of the Th chain, the most relevant isotope is ^{208}Tl ($T_{1/2}$ = 3.0 min, 36% branching ratio), which beta decays to ^{208}Pb with a Q value of 5.0 MeV. An α–β delayed coincidence can help in the reduction of the number of isotopes falling in the ROI. However, also in this case, the longer half life will result in a smaller rejection factor compared to the ^{214}Bi case.

In addition to the LAB+PPO cocktail purity, any material associated with the NLDBD loading must be considered. SNO+ reports a target level after the 0.5% Te loading of around 10^{-15} and 10^{-16} g/g for the U-238 and the Th-232 chains, respectively. KamLAND-Zen [22] reports a purity of $(1.3 \pm 0.2) \times 10^{-16}$ g/g U and $(1.8 \pm 0.1) \times 10^{-15}$ g/g Th. Higher purity levels are achievable by improving the target material purification technique, i.e the purity grade of the chemicals used to process the tellurium. A target purity of 10^{-17} g/g for both the U and Th chain has been assumed for the THEIA experiment. This purity level require a reduction factor of 99.9% of the ^{214}Bi events in the ROI in order to reduce the internal background to a negligible level. Factor 10 worse purity would require a factor 10 better background reduction. Both factors are within the level shown to be achievable by tagging techniques.

e. Balloon Backgrounds Among the external background sources, the closest to the target volume are the ^{214}Bi and ^{208}Tl decays in the containment balloon. A typical balloon material is nylon, and the intrinsic purity levels can be found in [23]. The values, based on Borexino measurements, are 1.1 ppt and 1.6 ppt for U and Th, respectively. KamLAND-Zen has also measured the purity level of the nylon they used for their balloon. Results in Reference [24] give 2 ppt and 3 ppt for U and Th, respectively. The purity levels reached by Borexino are used as target levels for the THEIA experiment. A nylon balloon with a thickness of about 435μm is assumed.

f. PMT Backgrounds For the present discussion it is assumed that with a fiducial volume cut the background induced by the PMTs is negligible in the region of interest for THEIA NLDBD studies.

3. NLDBD Sensitivity

a. Detector Modeling In order to study sensitivity to NLDBD in THEIA, the dominant backgrounds have been simulated using the Geant4-based RAT-PAC software package.[1] The detector is modeled as a cylinder with 20 m fiducial radius and 40 m height, for a total fiducial mass of 50 kt, located in the Homestake mine at a depth of 4300 m.w.e. A PMT coverage of 5% has been used for the simulations, then rescaled according to the assumed light yield.

[1] `https://github.com/rat-pac/rat-pac`

The model assumes a liquid scintillator contained in the balloon composed of LAB with 2 g/l PPO (density of 0.86 g/cm^3), while the volume outside the balloon is filled with a WbLS (10% LAB-PPO and 90% water). The optical properties of the LAB-PPO cocktail have been measured by the SNO+ collaboration. For the WbLS, the optical properties are obtained by weighting contributions of the LAB-PPO and water, and are consistent with benchtop measurements. A multi-component absorption and reemission model (i.e. separate absorption lengths and reemission probabilities for each of the cocktail component) are used in the simulation. Radioactive decays are simulated using the Decay0 code [27].

While event reconstruction algorithms remain under development, the reconstructed energy is approximated by assuming the Poisson limit of photon counting: the true deposited energy, accounting for quenching, is smeared out by a Gaussian resolution function corresponding to the light yield. As a baseline, an average light yield of 1200 PMT hits per deposited MeV is assumed (corresponding to about $3\%/\sqrt{(E)}$ energy resolution), except where noted. The used value takes into account the reduction of the light yield due to the addition of the isotope. The light yield for the pure scintllator would be 1800 Nhits/MeV or 2% at 1 MeV. For the Xe loaded scintillator, the used light yield is likely an underestimation as the KamLAND-Zen experiment predicts a reduction of only 15% in light yield at the reached 3% loading, which would correspond to 1600 Nhits/MeV [31].

b. Counting Analysis To estimate the sensitivity, a single-bin counting analysis is employed. Since all backgrounds do not scale with isotope mass (e.g. solar neutrinos and external γ backgrounds), we use the Monte Carlo to evaluate the background expectation, establish a confidence region using the Feldman-Cousins frequentist approach, and derive an expected limit on the NLDBD half life:

$$\widehat{T}^{0\nu\beta\beta}_{1/2}(\alpha) = \frac{N \cdot \epsilon \cdot t \cdot \ln 2}{\mathrm{FC}(n = b, b; \alpha)} \tag{19}$$

where N is the number of atoms of active NLDBD isotope, ϵ is the efficiency, t the live time, and b the expected background. 'FC' refers to a Feldman-Cousins interval at confidence level α.

The NLDBD region of interest is defined by a a fiducial volume cut and energy window. The fiducial volume is 7 m for an 8 m radius balloon, which reduces backgrounds from the balloon material. The energy window is asymmetric about the Q value, from $-\sigma/2 \rightarrow 2\sigma$ of a Gaussian fit to the NLDBD signal peak; this maximizes signal acceptance ($\epsilon = 66.9\%$) while removing much of the steeply-falling two-neutrino DBD background spectrum.

To summarize the baseline background assumptions detailed above, we use a reduction factor for ^{10}C of 92.5%, ^{214}Bi 99.9%, balloon backgrounds 50%, and ^{8}B solar neutrinos 50%.

	Events/ROI·y	
Signal	Te Loading	^{enr}Xe Loading
Loaded isotope mass [t]	31.4	49.5
$0\nu\beta\beta$ (10 meV)	108.9	116.4
$2\nu\beta\beta$	80.0	38.2
^{8}B Solar ES (50%)	138.5	138.4
^{10}C (92.5%)	24.6	25.4
^{130}I	80.5	—
^{130m}I	2.9	—
^{136}Cs	—	0.57
^{208}Tl	0.02	0.002
^{214}Bi (99.9%)	4.0	4.4
Balloon ^{214}Bi (50%)	24.0	27.4
Balloon ^{208}Tl (50%)	0.25	0.14
Total	354.8	234.5

TABLE II: Expected background counts per year in the ROI. In parenthesis is shown the reduction factor applied.

The expected event rates per year for a ^{nat}Te or ^{enr}Xe loaded THEIA detector with an 8 m radius containment balloon are given in Table II. For Xe we considered a loading at the level of 3% by mass, while for Te the considered loading is of 5% by mass. In the Xe case, enrichment to 89.5% ^{136}Xe is used, while Te is in its natural form (34.1% ^{130}Te). Figure 2 shows the background spectra near the endpoint in the Te (Figure 2a) and Xe (Figure 2b) cases.

Following Equation 19, we obtain a sensitivity in terms of $\hat{T}^{0\nu\beta\beta}_{1/2}$, and compute a corresponding limit on the effective Majorana neutrino mass $m_{\beta\beta}$ assuming a light neutrino exchange model with phase space factors from Kotila and Iachello [28] and using the IBM-2 matrix element [29] for definiteness (g_A=1.269). The 90% CL sensitivity is:

$$\textbf{Te}: \; T^{0\nu\beta\beta}_{1/2} > 1.5 \times 10^{28} \text{ y}, \; m_{\beta\beta} < 5.4 \text{ meV}$$

$$\textbf{Xe}: \; T^{0\nu\beta\beta}_{1/2} > 2.7 \times 10^{28} \text{ y}, \; m_{\beta\beta} < 4.8 \text{ meV}$$

Energy Resolution The sensitivity is strongly dependent on the energy resolution, which in turn depends on the total detected light yield, since this sets of the level to which events in the steeply-falling $2\nu\beta\beta$ decay spectrum can migrate into the NLDBD energy ROI. Figure 3a shows the impact, holding other assumptions fixed.

Solar Neutrinos It is possible in principle to discriminate solar neutrino interactions from NLDBD signal, using Cherenkov light to determine the direction with respect to the Sun and possibly separate one- and two-ring topologies, on a statistical basis if not event-by-event. This is particularly important for THEIA, where solar neutrinos are expected to be the largest background. Figure 3b shows the sensitivity scaling with solar neutrino event rejection.

U/Th Chain Backgrounds The level of internal and external U and Th chain background reduction also depends on the power of timing and topology-based particle identification methods. Figures 3c and 3d show the sensitivity as a function of the external background and ^{214}Bi reduction factors, respectively, with other parameters fixed.

4. Alternative Isotopes

Few alternative isotopes has been explored, which would be favorable in terms of annual abundance and costs. However, the shorter double-beta decay half-life, up to two orders of magnitude, and the small isotopic abundance is an extremely limiting factor in reaching a limit on the effective Majorana neutrino mass below 5 meV, even for light yield close to the pure scintillator ones.

The isotopes considered are ^{100}Mo, ^{82}Se and ^{150}Nd. A summary of the expected events in the 0NDBD ROI and the corresponding limits on the half-life and Majorana mass are given in Table III. The selected loading of 2% for Se and Nd is based on results of stability tests in table-top experiments. For Mo a loading up to 3% seems to maintain good stability and optical properties. In case of Nd an enrichment factor of 90% is considered. This is necessary to reach a competitive limit on the 0NDBD half-life. The enrichment option for Mo and Se is considered less promising than the Nd one, due to the smaller $G_{0\nu}M_{0\nu}^2$ value. The expected neutrino induced backgrounds (^{100}Tc for Mo, ^{82}Br for Se, and ^{150}Pm for Nd) are obtained considering the interaction rates given in [25, 26]. The scintillator purity is kept at 10^{-17}g/g for both U and Th for all the mixtures, unless otherwise noted.

Among the alternatives explored, the 2% enriched Nd cocktail is the only option providing a competitive limit on the effective Majorana neutrino mass, approaching the limit obtained with a 5% Te loaded scintillator for high light yield as shown in figure 4.

Signal	Events/ROI·y Se Loading	Mo Loading	^{enr}Nd loading
Loading fraction (%)	2	3	2
Isotope fraction (%)	8.73	9.82	90
Loaded isotope mass [t]	3.2	5.4	33.2
$2\nu\beta\beta$	117.3	325.6	2042
^{8}B Solar ES (50%)	136.2	135.6	132.9
^{10}C (92.5%)	9.91	8.49	0.28
^{100}Tc	—	0.34	—
^{82}Br	0.21	—	—
^{150}Pm	—	—	0.145
^{208}Tl	158.4	198.7	563.4
^{214}Bi (99.9%)	0.18	0.09	— (*)
Balloon ^{214}Bi (50%)	3.8	3.0	0.2
Balloon ^{208}Tl (50%)	31.7	31.0	50.5
Total	457.8	702.8	2789.9
Expected $T_{1/2}$ ($\times 10^{27}$ yr)	2.2	2.4	5.1
Expected mass (meV)	15.5	13.8	7.6

TABLE III: Expected background counts per year in the ROI. In parenthesis is shown the reduction factor applied. (*) Assumed 10^{-16} g/g in U. Limits on the effect Majorana neutrino mass are obtained for 90% C.L. (FC approach) with phase space factors from [28] and matrix elements from [29] (g_A=1.269).

5. Conclusions

In summary, the THEIA experiment can perform a very sensitive search for NLDBD, assuming a high level of Te or Xe loading and background levels near those demonstrated by previous experiments. We have performed a single-bin sensitivity analysis considering the dominant backgrounds for an experiment located at the 4850 foot level of Homestake, accounting for solar neutrino interactions, cosmogenic activation, and radioisotopic contamination of detector materials. We have studied the behavior of these backgrounds using a microphysical Monte Carlo simulation with a detector model including scintillator and WbLS optics. We find that for aggressive assumptions of radiopurity and background rejection, a THEIA NLDBD search is capable of reaching sensitivity within the non-degenerate normal hierarchy parameter space.

E. Geoneutrinos - S Dye for antinu group

F. Sterile Neutrinos - volunteers?

a. Motivation BRIEF intro to physics motivation, and status of the field: our major competitors

b. XX with THEIA What we bring to the table - pros of THEIA design

Sensitivity estimates with baseline design (one of THEIA i–iii)

c. Detector Requirements A summary of the impact of different detector choices i.e. what happens if we stray from the relevant baseline

G. Solar Neutrinos - GDOG, R Bonventre

Both water Cherenkov and liquid scintillator detectors have a long history of successful observation of solar neutrinos. A number of open questions remain, including: first detection of neutrinos from the sub-dominant CNO fusion cycle, as a method to resolve the solar metallicity; a precision probe of the transition region between low-energy vacuum-dominated oscillation, below 1 MeV, and matter-dominated regime above 5 MeV, as a sensitive search for new physics effects; tests of solar luminosity through precision measurements of pep and pp neutrinos; tests of the solar temperature and, potentially, separation of the different components of the CNO flux to probe the extent to which this cycle is in equilibrium in the Sun's core.

Many of these questions can be addressed by THEIA's combination of a low-threshold directional detector, along with the potential for isotope loading. THEIA would provide unprecedented sensitivity to solar neutrinos via two channels:

1. *Huge statistics for elastic scattering (ES) events at low energy.* The LENA collaboration [**?**] have explored in detail the power of a large-scale scintillator detector for resolving open questions in solar neutrino physics, such as determining the solar metallicity via a measurement of neutrinos from the sub-dominant CNO fusion cycle. THEIA would have similar capability, along with the additional advantage of being able to distinguish ES events from backgrounds (such as ^{210}Bi) using directionality.

2. *Potential charged-current (CC) detection via isotope loading e.g.* ^{7}Li [**?**]. The differential CC cross section for neutrino interaction on ^{7}Li is extremely sharply peaked. As a result, CC neutrino detection provides a high-precision measurement of the incoming neutrino energy, allowing extraction of the low-energy ^{8}B spectrum. This would provide a sensitive search for

	H2O Level (g/gH2O)	LS Level (g/gLAB)
^{238}U Chain	6.63e-15 [**?**]	1.6e-17 [**?**]
^{232}Th Chain	8.8e-16 [**?**]	6.8e-18 [**?**]
^{40}K	6.1e-16[a]	1.3e-18 [**?**]
^{85}Kr	2.4e-25[b]	2.4e-25 [**?**]
^{39}Ar	2.75e-24[b]	2.75e-24 [**?**]
^{210}Bi	3.78e-28[b]	3.78e-28 [**?**]
^{11}C	0	1.0e5 (ev/kT/year) [**?**]

TABLE IV: Background assumptions for the baseline configuration.
[a] The ^{40}K level in water is taken to be 0.1x the Borexino measurement [**?**]
[b] The ^{85}Kr, ^{39}Ar, and ^{210}Bi levels in water are taken to be the Borexino measured level in scintillator [**?**], although levels increased by several orders of magnitude are explored

new physics via a probe of the transition region in the neutrino spectrum between vacuum-dominated and matter-enhanced oscillations. There is also the potential to separate the different components of the CNO flux via a shape analysis.

1. ES Measurements

The sensitivity to CNO and pep solar neutrinos of an unloaded WbLS detector via the ES interaction has been studied in [**?**].

By performing a two-dimensional binned maximum likelihood fit in energy and direction relative to the Sun, $\cos\theta_\odot$, neutrino fluxes are separated from each other, as well as from certain sources of radioactive background. For each signal the $\cos\theta_\odot$ distribution was determined fully analytically. All non-neutrino signals were assumed to be flat. For the solar signals the electron direction relative to the Sun was determined based on the differential cross sections. This was then convolved with a chosen angular resolution. The energy response was determined semi-analytically, based on chosen detector parameters such as target light yield and photocathode coverage. This paper summarises the assumptions made regarding detector configuration and performance, and the resulting sensitivity to solar neutrinos. Full details of the analysis are described in [**?**].

The baseline detector configuration was chosen to be a 50-kT detector with 90% PMT coverage, a 5% WbLS target, and 25° angular resolution, with baseline background levels as given in Table IV. The dominant cosmogenic background, from ^{11}C, was conservatively taken to be at the Borexino level, scaled by the respective target mass. If located at the proposed site at LBNF this background would in fact be significantly lower. All results assume a five year livetime.

The impact of each choice of detector configuration and background level was studied, including

Signal	Normalization sensitivity (%)
^{8}B ν	0.4
^{7}Be ν	0.4
pep ν	3.8
CNO ν	5.3
^{210}Bi	0.1
^{11}C	11.5
^{85}Kr	10.5
^{40}K	0.04
^{39}Ar/^{210}Po	21.9
^{238}U chain	0.02
^{232}Th chain	0.05

TABLE V: Fit uncertainty for 5 years of data with the baseline configuration and background assumptions

the target mass, the percentage loading of LS in the WbLS target, photocathode coverage, angular resolution, and background levels. Energy reconstruction was performed semi-analytically, and the resolution was determined from a combination of the target light yield and photocathode coverage. The effect of systematic uncertainties in both energy scale and resolution were considered. A full reconstruction of event direction was not attempted; rather, the impact of certain values of angular resolution was considered. In practice, the achievable angular resolution would be correlated with other detector parameters, such as the percent LS loading – a higher fractional loading makes separation of the prompt Cherenkov signal from the isotropic scintillation more challenging, thus limiting the angular resolution. This separation could be further enhanced by deploying fast photon sensors, such as LAPPDs [**?**].

The fit uncertainty for each signal with the baseline detector configuration and background assumptions is shown in Table V.

The impact on the CNO solar neutrino sensitivity of detector size, LS fraction, and angular resolution for the baseline background assumptions is shown in Table VI and Fig. 5.

A study of both energy scale and resolution systematics shows that these can be constrained by the data to sub-percent levels, making them sub-dominant in the final flux sensitivities.

The sensitivity was shown to be extremely robust to background level variations of several orders of magnitude at the baseline angular resolution, and to the assumed level of $\beta - -\alpha$ discrimination and BiPo coincidence rejection. Even the dominant background to the Borexino measurement, ^{11}C, was shown to have a small impact, demonstrating that the depth of the experiment site is not a critical factor. This is to be expected, since the directional resolution provides extremely strong separation between solar neutrino signal events and the uniform background events. The level of ^{40}K was observed

Target mass	WbLS	Angular resolution			
		25°	35°	45°	55°
50 kT	0.5%	6.2	8.8	11.2	13.5
50 kT	1%	6.1	8.7	11.0	13.4
50 kT	2%	6.2	8.9	11.4	13.8
50 kT	3%	5.9	8.4	10.7	13.0
50 kT	4%	5.5	7.9	10.1	12.3
50 kT	5%	5.3	7.6	9.7	11.8
25 kT	0.5%	8.5	12.2	15.6	18.7
25 kT	1%	8.5	12.1	15.0	18.4
25 kT	2%	8.5	12.1	15.5	18.7
25 kT	3%	8.0	11.5	14.6	17.7
25 kT	4%	7.6	10.9	13.9	16.8
25 kT	5%	7.3	10.5	13.3	16.2

TABLE VI: CNO flux sensitivity (%) as a function of target mass, WbLS % and angular resolution for 5 years of data with 90% PMT coverage and the baseline background assumptions

to have the largest impact: an increase of x10 in this background reduces the CNO sensitivity by a factor of 2. ^{40}K is a dominant background at low energies. This is due to the much higher contamination in the water component of the WbLS compared to the relatively cleaner scintillator – even assuming an order of magnitude improvement over the level measured in water by Borexino and SNO. The ^{40}K background in water was not critical for these previous measurements, and so it may be possible to further reduce the level with additional effort. The SNO water processing plant could be improved by increasing the frequency of replacing ion exchange columns or by distilling the water. A successful measurement in WbLS would rely on such improvements.

2. CC Measurements

The potential for CC measurements in Theia was studied in [**?**]. That work is summarised here.

Several factors contribute to the choice of isotope for loading into a scintillator detector. ^{37}Cl and ^{71}Ga have been used successfully by radiochemical experiments from the late 1960s to the present day. ^{7}Li has been considered as a favorable alternative [**?**] but such a detector was never constructed. ^{7}Li was also proposed as an additive to a water detector in [**?**]; such a detector would have excellent sensitivity to the high end of the ^{8}B spectrum, but would be limited in threshold. As seen in Fig. 6, ^{71}Ga and ^{7}Li both have more favorable cross sections than ^{37}Cl, particularly at low energies. However, the cost of ^{71}Ga would likely be prohibitive in a liquid scintillator experiment. The relatively large differential uncertainties on the ^{71}Ga cross section would also smear out any extracted spectrum whereas the cross sections on ^{37}Cl and ^{7}Li are known to extremely high precision. The ^{37}Cl cross section has

been mapped using the β decay of ^{37}Ca. The CC interaction of ν_e on ^{7}Li is shown in Eq. (20).

$$^7Li + \nu_e \rightarrow {}^7Be + e^- \quad (\mathrm{Q} = 862 \text{ keV}) \tag{20}$$

^{7}Li has only two significant transitions: a mixed Fermi and Gamow-Teller transition to the ground state of ^{7}Be with a threshold of 0.862 MeV; and a super-allowed Gamow-Teller transition to the first excited state at ∼430 keV, which decays with a lifetime of τ ∼200 fs. The scattering is very hard, transferring almost all incident energy to the scattered electron. If one could differentiate between the electron of the ground state and the $e^- + \gamma$ of the first excited state one would have a high-precision reconstruction of neutrino energy. The two states also have precisely known angular distributions, which could then be used as an additional handle to differentiate signal from background. Even without the use of particle ID to differentiate between states the contribution of the two is known precisely from theory, so the difference in threshold can be used to demonstrate that the two are being seen in the correct proportions. There is also the potential to observe NC interactions on ^{7}Li (Fig. 6), exciting the analog 478 keV first excited state of ^{7}Li, which then decays with a lifetime of τ ∼105 fs. On preliminary investigation ^{7}Li would thus appear to be the preferred isotope. However, other factors may be important, such as the effect of isotope loading on scintillator optics.

Figure 7 shows the predicted spectrum for the THEIA detector assuming a 30-kT fiducial volume loaded with 1% ^{7}Li by mass, and a conservative light yield of 100 photoelectrons per MeV. Standard MSW oscillation is assumed. Solid lines show the CC interactions and dashed lines show ES detection. The ES statistics by far outweigh the CC (as expected at a low %-level loading); however, the use of directionality would allow excellent separation. The right-hand panel shows the spectrum with a cut placed on $\cos\theta_\odot = 0.4$ (where $\theta_\odot$ is the angle between the event direction and a vector pointing back to the Sun), which reduces the ES signals by more than 2 orders of magnitude. (Angular resolution equivalent to SK-III was assumed). In practice a more sophisticated analysis would link the normalization of the ES and CC neutrino signals via their known cross sections, allowing the ES to be used to separate events from radioactive and cosmogenic backgrounds such as ^{210}Bi and ^{11}C, and the CC to provide the spectral sensitivity. The power of the CC signal can be observed in particular in the ^{8}B spectrum, which has a distinctive shape, and the strong peak in the *pep* signal in comparison to the broad ES spectrum.

Due to limited sensitivity, experiments to date have only considered detection of the sum of the three CNO lines. The increased spectral sensitivity from isotope-loaded WbLS could allow the possibility to separate the constituent lines of the CNO neutrino flux. The CNO cycle depends critically on

temperature in the conversion of C to N, reaching equilibrium only in the most central region of the solar core, where $T > 1.33 \times 10^7$ K. In this region, equal numbers of neutrinos are produced in the β^+ decay of ^{13}N and ^{15}O, whereas in the cooler outer regions only ^{13}N neutrinos are produced. Independent measurements of the ^{13}N and ^{15}O neutrino fluxes would determine the separate primordial abundances of C and N [**?**]. Figure 8 shows the predicted CNO spectrum broken into its individual components. A sufficiently sensitive detector with a low enough threshold could separate the contributions from ^{13}N and ^{15}O. A separate measurement of ^{17}F is unlikely due to the much lower flux; however, there is a strong theoretical basis for fixing the ^{17}F component to a known fraction of the sum of ^{13}N and ^{15}O.

H. Supernova Neutrinos – Michi Wurm

The neutrino burst detected from the next galactic Supernova will provide us with a wealth of information on the dynamics of the core collapse (neutronization, reheating, proto-neutron star cooling) and the properties of the neutrinos themselves (mass hierarchy, absolute mass scale, collective oscillations). Since the first detection of Supernova neutrinos in 1987, the scientific community has not become tired to predict new effects and their signatures that are potentially to be extracted from the neutrino signal. So while we are uncertain what to expect from the next event and how different effects will overlay, it is beyond doubt that only a concerted effort making use of the complementary strengths of all the neutrino observatories available will enable us to extract the full amount of information. Moreover, this combined analysis has to reach beyond neutrino detectors, including gravitational wave and (if present) optical signatures to appreciate the full picture.

If a Supernova neutrino burst would pass by the Earth today, hundreds of events would be expected in several smaller observatories (LVD, Borexino, KamLAND, SNO+, HALO to name but a few). However, the largest event statistics would be collected by the two large Cherenkov detectors, Super-Kamiokande (SK) and IceCube. Ten years from now, we may expect that two further players will appear on the stage: JUNO offering a liquid scintillator target, and DUNE allowing SN neutrino detection in liquid argon. In the most simplified picture, SK, JUNO and IceCube will dominate the information on $\bar{\nu}_e$ flux and energies, while DUNE has the potential for a high-statistics ν_e measurement. JUNO will provide information on the combined flux of ν_μ and ν_τ and antineutrinos (in the following, we use the conventional denotation ν_x).

1. Detector Configuration

In the following, we assume the THEIA-ii detector configuration, i.e. a 50 kt neutrino target filled with a WbLS containing 10 % of organic scintillator. With 90 % optical coverage, the expected photoelectron yield for a 10 %-WbLS is ∼200 p.e./MeV (75 % scintillation), providing a stochastic energy resolution of 7 %. Thus, THEIA will provide a threshold in the low MeV range and − given the high coverage − spectroscopic capabilities close to that of current-day organic liquid scintillator detectors. Importantly, THEIA will provide a clear neutron tag, allowing to discriminate Inverse Beta Decay (IBD) events from other single-event backgrounds.

Given this additional features, what can THEIA add to the global picture of SN neutrino observations?

- a high-statistics IBD ($\bar{\nu}_e$) signal, offering considerably better energy resolution than SK and about twice its statistics; both will prove very useful when trying to correlate spectral features changing over time with other signals, e.g. gravitational wave emission during the SASI phase, or when looking for energy-dependent oscillation patterns (e.g. the spectral swaps induced by collective oscillations)

- improved pointing accuracy for the ν_e elastic scattering signal, improving the current day ∼3° resolution of SK to the level of 1° or better. The key is the almost complete event-by-event subtraction of IBD events enabled by the neutron capture tag [**?**]; SK+Gd can expect a similar improvement but offers a neutron tagging efficiency of only ∼70 %

- the chance to glimpse the initial ν_e neutronization burst [**?**]: however, as $\mathcal{O}(10)$ events are expected for a SN at 10 kpc, detailed information can only be expected for a relatively nearby Supernova

- relative to SK and JUNO, a $\bar{\nu}_e$ detector on the other side of the Earth, allowing to study Earth matter effects in $\bar{\nu}_e$ in a direct spectral comparison; note that, again, energy resolution is a key parameter here.

2. Spectroscopy of SN neutrinos in THEIA

Compared to all other running and upcoming detectors (except Hyper-Kamiokande), 50 kt of WbLS will constitute the largest neutrino target, roughly doubling the available statistics of IBDs in water (SK) and scintillator (JUNO) detectors. Moreover, THEIA will provide both good energy and directional resolution, offering handles to discriminate between different neutrino reaction channels.

As stated above, present knowledge of the SN neutrino emission and neutrino properties does not allow for a precise prediction of the expected signal. Nevertheless, to provide a scale of the expected signal we list in table VII the time-integrated event rates for a Supernova in 10 kpc distance (close to the galactic center), using energies and fluxes predicted by the GVKM (Gava-Kneller-Volpe-McLaughlin) model [**?**] and the cross-sections provided by the SNOwGLoBES framework.

Channel		Reaction	Event rate
Inverse Beta Decay	(IBD)	$\bar{\nu}_e + p \rightarrow n + e^+$	9,900
Electron Scattering	(ES)	$\nu + e \rightarrow e + \nu$	480
CC on ^{16}O	($\bar{\nu}_e$O)	$\nu_e + {}^{16}\mathrm{O} \rightarrow {}^{16}\mathrm{F} + e^-$	170
	(ν_eO)	$\bar{\nu}_e + {}^{16}\mathrm{O} \rightarrow {}^{16}\mathrm{N} + e^+$	220
NC on ^{16}O	(NC)	$\nu + {}^{16}\mathrm{O} \rightarrow {}^{16}\mathrm{O}^* + \nu$	550

TABLE VII: Neutrino event rates expected in 50 kt of WbLS (10 % scintillator) for a core-collapse Supernova at 10 kpc distance. Neutrino spectra and fluxes follow the GVKM model [**?**].

Event rates. The signal is vastly dominated by the $\bar{\nu}_e$-induced IBD events, followed by the NC reactions of all neutrino flavors on oxygen and elastic scattering off electrons. Note that as WbLS contains as well carbohydrates, THEIA will detect relevant numbers of neutrino events on carbon: For a 10 % WbLS, ∼250 events from NC carbon reactions are expected, inducing a gamma peak at 15 MeV (not shown in fig. 9), adding to the information on the integrated neutrino flux.

Energy spectrum Given its large target mass and good energy resolution, THEIA will offer detailed spectral information for the $\bar{\nu}_e$ flux (based on IBD events). Moreover, less precise but still relevant spectral data will be available for all other neutrino flavors that are detected in their hundreds. In figure 9, we show the expected event spectra as a function of their visible energy, already smeared with a 7 % energy resolution. As for the rate, the IBD signal dominates the interaction rates for all energies, with the noteworthy exception of the two low-energy γ lines from the NC reaction on oxygen. However, differently from current-day water Cherenkov detectors, the neutron tag for IBD events allows to subtract the IBD signal on an event-by-event basis, providing better access for a separate study of the subdominant reaction channels. As a consequence, the gamma lines from the NC reaction are easy to extract from the remaining spectrum, providing a flavor-independent measurement of the neutrino flux [**? ?**]. Moreover, the presence of scintillation light and high energy resolution enables separate detection of the strongest gamma lines and thus a measurement of their relative spectral contributions. In case of a very efficient IBD subtraction (close to 100 % efficiency), there will be even some potential to separate the remaining ES, ν_eO and $\bar{\nu}_e$O channels: ES events are strongly correlated with the SN direction and will stand out in any case (see below). Moreover, the re-decay of ^{16}N potentially offers a

delayed coincidence signature for $\bar{\nu}_e$O events: The remaining ν_eO would then provide access to a small but pure sample of electron neutrino events.

Time-dependent features A time-dependent measurement of the neutrino signal is especially interesting for studying the different phases and physical processes underlying the core collapse. For a Supernova in 10 kpc distance, the initial neutronization burst will translate only to a small number of ES and ν_eO events in THEIA, $\mathcal{O}(10)$. However, if the SN were to happen closer and if the information of several detectors (especially DUNE) is combined, energy, flux and flavor content may be studied in detail. On its own, THEIA will provide detailed spectral information of the $\bar{\nu}_e$ flux during the accretion phase, nicely complementing the flux information available from IceCube.

SN neutrino pointing. In Water Cherenkov Detectors like SK, the direction of the incoming neutrino burst can be determined based on the recoil electrons from ES: Given the relatively large neutrino energies, the electrons are very tightly aligned with the initial momentum of the neutrino. In SK, this will be sufficient to pinpoint the location of the SN within 3-4 degrees [**?**]. The most important factor limiting resolution in this case is the relatively high background formed by the only slightly directional positrons from IBD interactions. In the angular distribution of events, a peak consisting of $\sim 10^2$ ES events has to be found over a flat background of several thousand IBDs.

It has been suggested (e.g. in [**?**]) that the directional resolution can be considerably enhanced if the IBD events can be discriminated based on the delayed neutron tag, reducing the flat background. This represents one of the key features of SN neutrino detection in THEIA: As an example, the left panel in figure 10 shows the angular distribution for an SN neutrino burst (Wilson model [**?**], 10 kpc distance), where an efficiency of 90 % is assumed for IBD rejection: While the ES events are clearly peaked in the direction of the SN ($\Delta\theta = \Delta\phi = 0°$), the reduced IBD background constitutes only a minor background noise.

We studied the effect of IBD background reduction on the directional resolution based on a toy MC of the signal. For this, we fitted the output angular distribution with a radial exponential plus flat background resolution, regarding three different cases: No, 90 % and full IBD reduction with full detection efficiency for ES events. For the latter, we considered full event kinematics (linking electron and neutrino momentum directions) and an intrinsic angular resolution of 10°. The results are depicted in the right panel of figure 10, once for a fiducial mass of 45 kt in the THEIA-ii configuration where close to full detection efficiency for the delayed neutron tag can be assumed, and once for half this mass to allow for an easier comparison to current SK pointing capabilities. While we can reproduce the $\mathcal{O}$(3-4°) pointing accuracy of SK, THEIA will reach an angular resolution of close to 1°.

It should be noted that SK+Gd will feature as well improved pointing precision based on the available delayed neutron tag. For this case, angular resolution can be estimated to $\sim 2^{\circ}$.

I. Diffuse Supernova Neutrino Background - S Dye for antinu group

J. Indirect Dark Matter ??

From Michi – there is still some interest in detecting decay/annihilation neutrinos in the multi-MeV range where THEIA would probably be able to place very competitive limits (as I noticed speaking to a theorist from Brussels a few weeks ago). It would be an addition to the antineutrino WG. Certainly, it?s rather low priority, but we could put it there as a place-holder.

IV. CONCLUSIONS

THEIA offers a broad program of compelling science, covering topics in nuclear physics, high-energy physics, astrophysics, and geophysics. These include: solar neutrinos and neutrinoless double beta decay; proton decay and long-baseline physics; supernova neutrinos and DSNB; and geoneutrinos, respectively.

Use of the novel, potentially inexpensive WbLS target allows construction of a precision detector on a massive scale. Successful identification of Cherenkov light in a scintillating detector would result in unprecedented background-rejection capability and signal detection efficiency via directionality and sub-Cherenkov threshold particle identification. This low-threshold, directional detector could achieve a fantastically broad physics program, combining conventional neutrino physics with rare-event searches in a single, large-scale detector. The flexibility of the WbLS target, of the options for isotope loading, and even of the detector configuration is a crucial aspect of THEIA's design. As the field evolves, THEIA has the unique ability to adapt to new directions in the scientific program, making it a powerful instrument of discovery that could transform the next-generation of experiments.

The feasibility of a low energy solar neutrino measurement with a large WbLS detector depends on the backgrounds and angular resolution achievable. At currently measured levels, the limiting background appears to be ^{40}K in water. Remaining backgrounds in water have little effect if they are kept to 1000 to 10000 times the level achieved in scintillator. The ^{11}C background has a small effect, which suggests that the overburden does not matter for this measurement. The impact of changes in scintillator and PMT coverage on energy resolution have relatively small effects, suggesting that even at 0.5% scintillator fraction, energy resolution is no longer the critical parameter to optimize. Instead,

the impact of these changes on threshold and angular resolution will be the deciding factor. With a baseline detector of 50-kT total volume (50% fiducial), 90% PMT coverage and a 5% WbLS target, assuming a 25° angular resolution, a precision of several percent is possible for both CNO and pep neutrino fluxes.

Further studies hinge on additional R&D, including the Cherenkov detection efficiency enhancement provided by deployment of fast photon sensors, and demonstration of quenching and particle ID capabilities in WbLS. Development of a directional reconstruction algorithm would allow a direct demonstration of the required angular resolution discussed in this article. An exciting avenue for further exploration would be isotope loading of the WbLS target, which would allow sensitivity to the low-energy spectral shape.

---

[1] M. Yeh *et al.*, "A New Water-based Liquid Scintillator and Potential Applications." Nucl. Inst. & Meth. A**660** 51 (2011).

[2] N. Rossi, Neutrino 2016 Conference, London, 3—10 July 2016, `http://neutrino2016.iopconfs.org/IOP/media/uploaded/EVIOP/event_948/14.00__1_.pdf`

[3] D. M. Mei et al., Astropart. Phys. 31, 417–420 (2009).

[4] L. Baudis et al., Eur. Phys. J. C 75, 485 (2015).

[5] C. Zhang et al., Astropart. Phys. 84, 62–69 (2016).

[6] E. B. Norman et al., Nucl. Phys. B (Proc. Suppl.) 143, 508 (2005).

[7] D.W. Bardayan et al., Phys. Rev. C 55, 820 (1997).

[8] B.S. Wang et al., Phys. Rev. C 92, 024620 (2015).

[9] V. Lozza and J. Petzoldt, Astropart. Phys. 61, 62–71 (2015).

[10] S. Andringa et al., Advances in High Energy Physics 2016, 6194250 (2016).

[11] C. Galbiati, A. Pocar, D. Franco, A. Ianni, L. Cadonati, S. Schoenert, Phys.Rev. C 71 055805 (2005).

[12] Y Gando, Nuclear and Particle Physics Proceedings, vol. 273- 275, pp. 1842-1846 (2016).

[13] T. Hagner et al., Astro. Phys. 14, 33–47, (2000).

[14] D. M. Mei and A. Hime, Phys. Rev. D 73, 053004 (2006).

[15] K. Zbiri, arxiv:0910.3714v3 [hep–ph] (2010).

[16] Borexino Collaboration, G. Bellini et al., JCAP08 49 (2013).

[17] SNO Collaboration, B. Aharmim et al., Physical Review C 88, 025501 (2013).

[18] C. Alduino et al., Eur. Phys. J. C 77 (2017).

[19] J.B. Albert et al., Phys. Rev. C 89, 015502 (2014).

[20] KamLAND Collaboration, K. Eguchi et al., Physical Review Letters 90, 021802, (2003).

[21] Borexino Collaboration, C. Arpesella et al., Physical Review Letters 101,091302, (2008).

[22] A. Gando et al. Phys. Rev. Lett. 110, 062502 (2013).

[23] https://www.radiopurity.org/rp/rp/_design/persephone/index.html?all

[24] I. Shimizu, Frontiers of liquid Scintillator Technology (FroST16), March 18, 2016 https://indico.fnal.gov/getFile.py/access?contribId=45&sessionId=25&resId=0&materialId=slides&confId=10355

[25] H. Ejiri and S. R. Elliott, Phys. Rev. C 89, 055501, (2014).

[26] H. Ejiri and S. R. Elliott, Phys. Rev. C 95, 055501 (2017).

[27] O.A.Ponkratenko, V.I.Tretyak, Yu.G.Zdesenko, Phys. At. Nucl. 63, 1282 (2000) (nucl-ex/0104018)

[28] Kotila, J., & Iachello, F. (2012). Phase-space factors for double-β decay. Physical Review C - Nuclear Physics, 85(3), 034316. http://doi.org/10.1103/PhysRevC.85.034316

[29] Barea, J., Kotila, J., & Iachello, F. (2013). Nuclear matrix elements for double-β decay. Physical Review C - Nuclear Physics, 87(1).

[30] KamLAND-Zen Collaboration, Phys. Rev. Lett. 117, 082503 (2016).

[31] Yoshihito Gando, Present Status of KamLAND-Zen, talk on International Workshop on Double Beta Decay and Neutrinos, Nov. 2011.

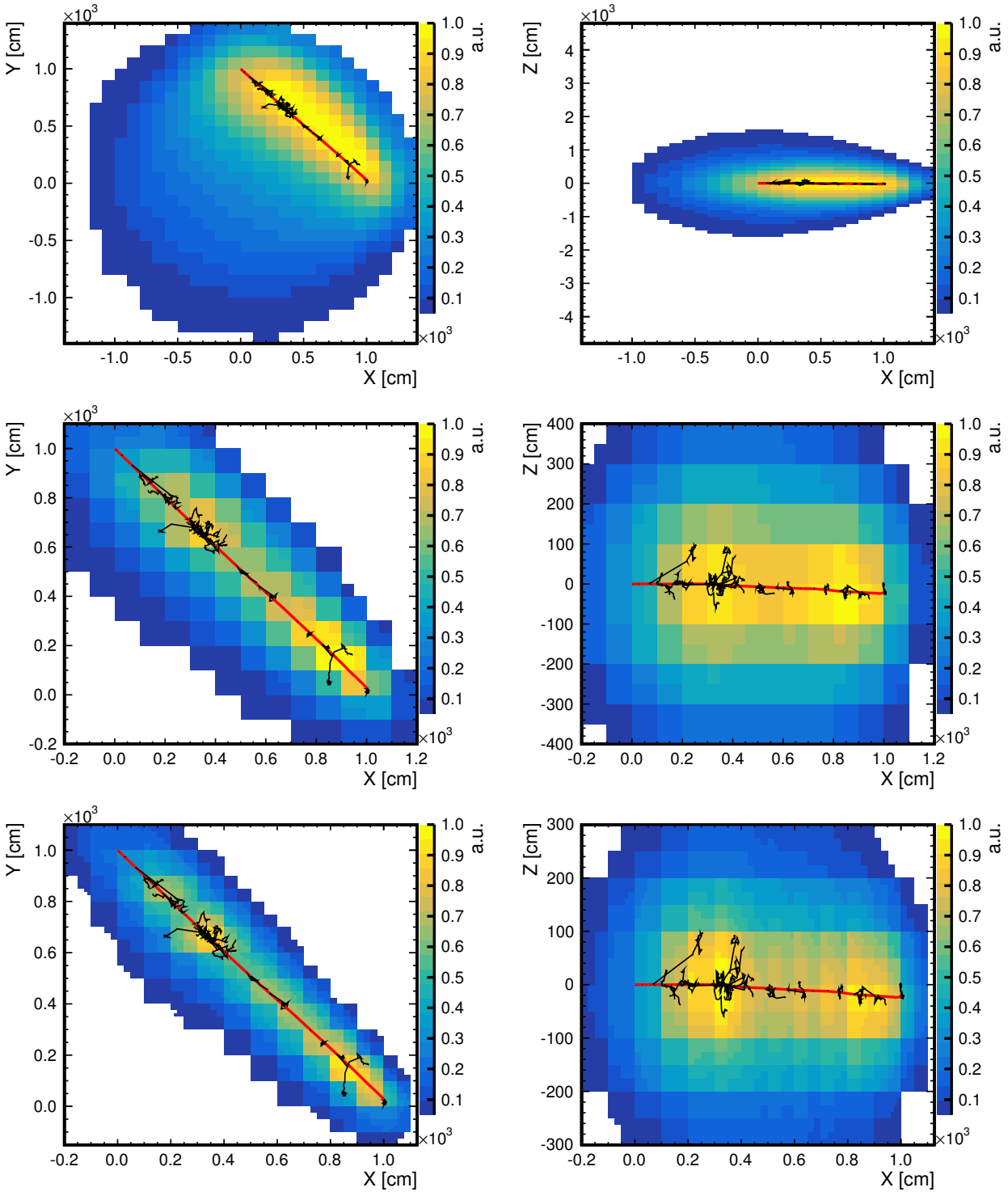

FIG. 1: Reconstruction results after the iterations 0 (top), 8 (middle) and 21 (bottom) for a simulated muon with 3GeV initial kinetic energy in the cylindrical LENA detector projected along the symmetry axis (left) or a radial y-axis (right). The primary particle started at (0, 1000, 0)cm in the direction (1, −1, 0). Both the projected tracks of the primary particle (red) and of secondary particles (black) are shown. Note that both the axis scales and the sizes of the cells change due to the selection of a region of interest and the refinement of the reconstruction mesh. Moreover, the cell content is given in a.u. and rescaled such that the maximum content is 1. Some details on the actual reconstruction procedure are given in sec:Reconstruction.

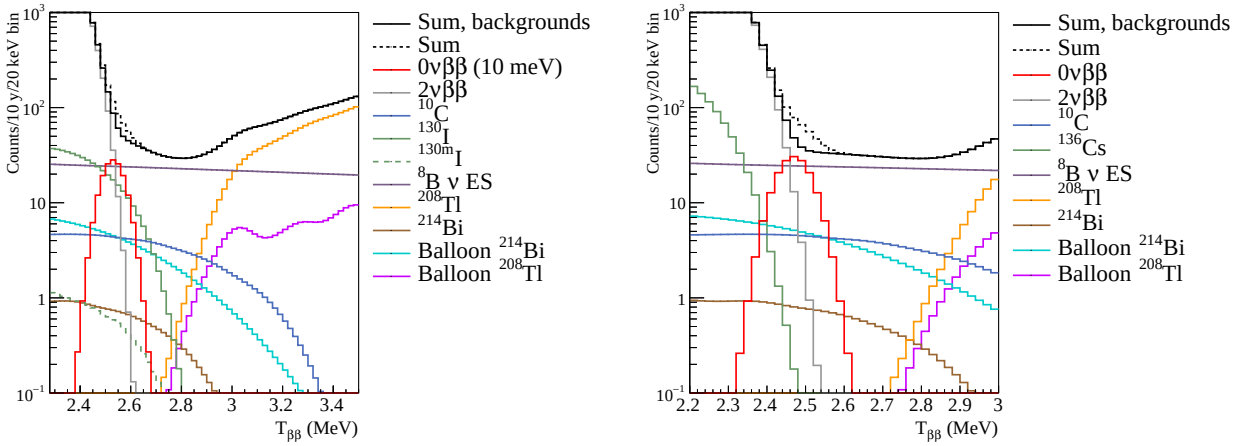

(a) Te loading

(b) Xe loading

FIG. 2: Energy spectra near the NLDBD endpoint for events within the 7 m fiducial volume.

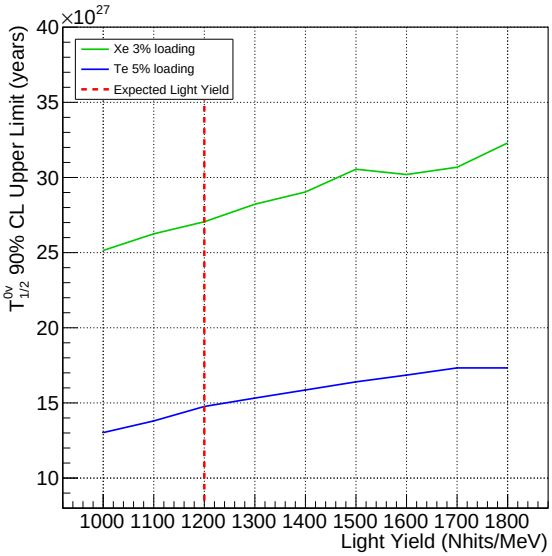

(a) Total detected light yield

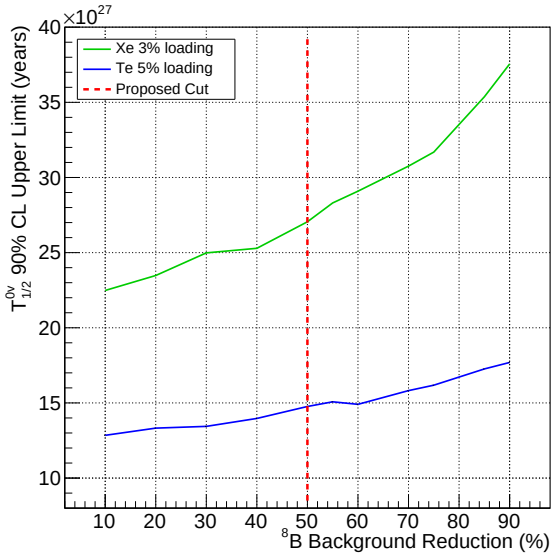

(b) Reduction factor for ^{8}B solar neutrinos

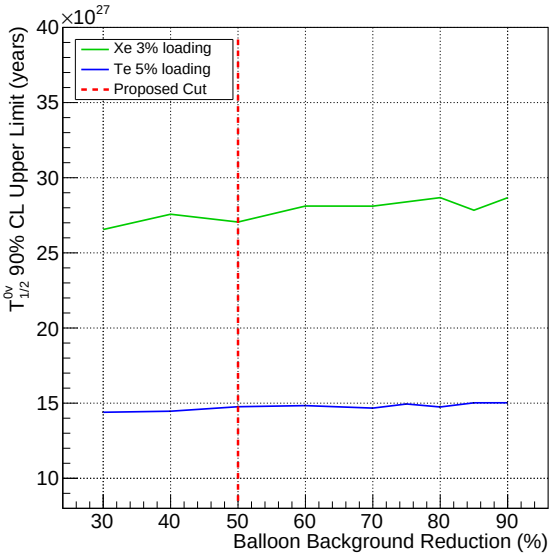

(c) Reduction factor for external backgrounds

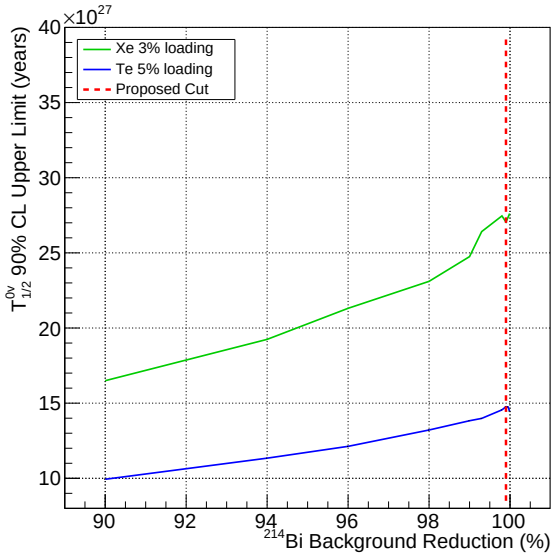

(d) Reduction factor for ^{214}Bi

FIG. 3: Mass sensitivity as a function of key experimental parameters.

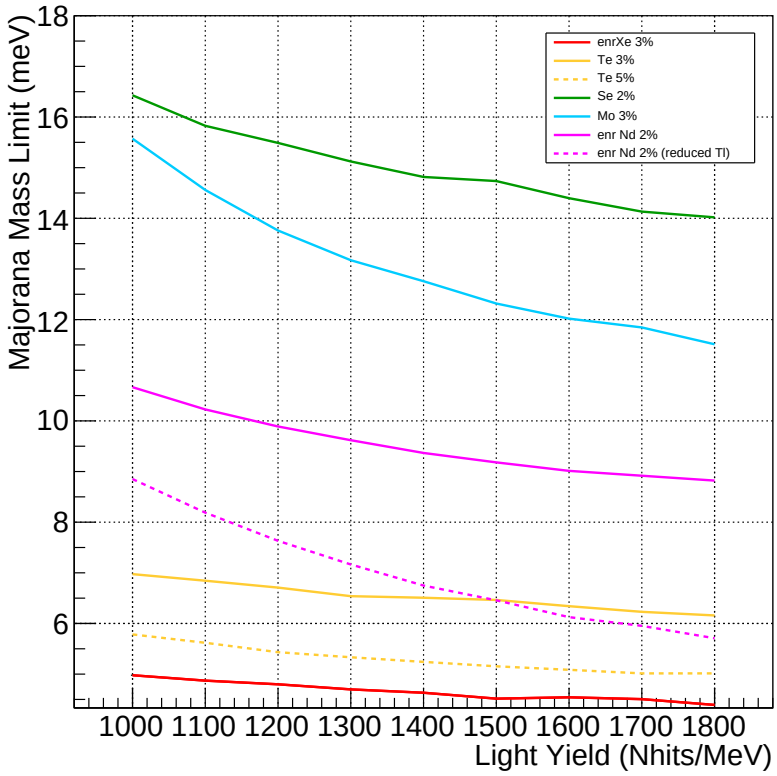

FIG. 4: Comparison plot for various loading and isotopes. Shown is the limit on the effective Majorana neutrino mass as a function of the light yield. 3%-^{enr}Xe loading still has the best limit, however 5% Te and 2%- ^{enr}Nd are a competitive option.

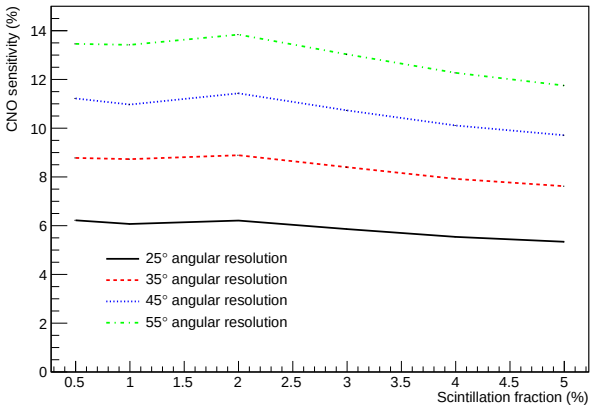

FIG. 5: CNO sensitivity as a function of scintillator fraction and angular resolution for a 50 kT detector after 5 years of running with the baseline background assumptions

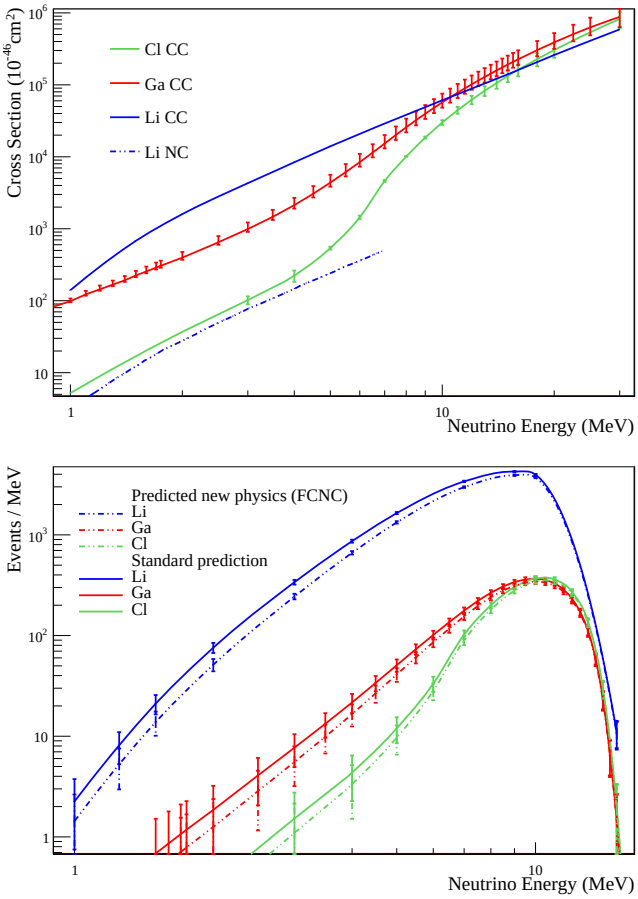

FIG. 6: (Top) The cross section for CC neutrino interaction on ^{37}Cl (green), ^{71}Ga (red), and ^{7}Li (blue) targets and NC on ^{7}Li (blue dashed). Data taken from [**?**], [**?**], [**?**], and [**?**], respectively. Although the differential uncertainties are not shown, the uncertainty on the lithium cross section is roughly 1% [**?**]. (Bottom) Predicted solar neutrino event spectra for 5 years of data-taking, with 1% loading by mass of candidate isotopes in a 30-kT WbLS-filled ASDC detector. Solid lines show the standard solar neutrino oscillation prediction. Dashed lines are for a flat neutrino spectrum to low energies, indicative of new physics interactions. ^{7}Li is the most favorable choice due to a high cross section for neutrino absorption. Five years of data taking results in over 17 σ separation in the integral flux, and correspondingly high precision (several σ significance) on the extracted spectrum.

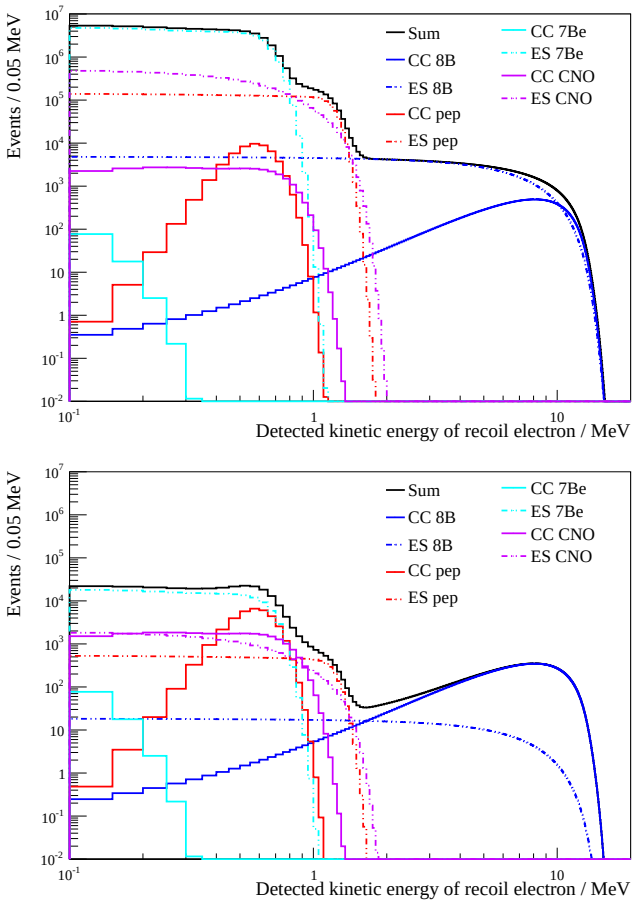

FIG. 7: (Top) Predicted solar neutrino spectra in a 30-kT WbLS-filled ASDC detector loaded with 1% ^{7}Li by mass. Light yield of 100 p.e./MeV assumed. (Bottom) The same spectra with a cut on $\cos\theta_{\odot} = 0.4$, reducing the ES component to illustrate the power of CC detection.

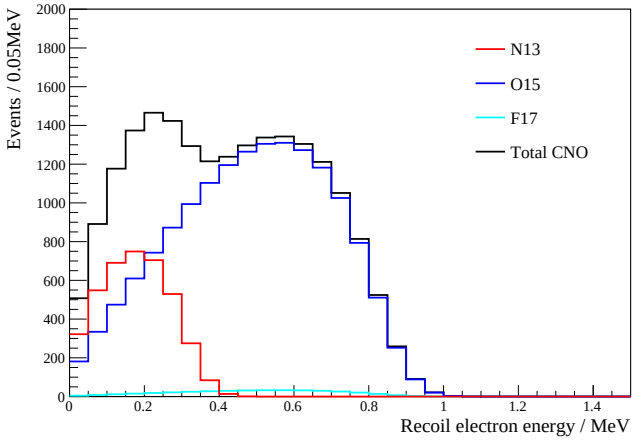

FIG. 8: Predicted spectrum for the individual components of the CNO neutrino flux, and the total, in a WbLS detector.

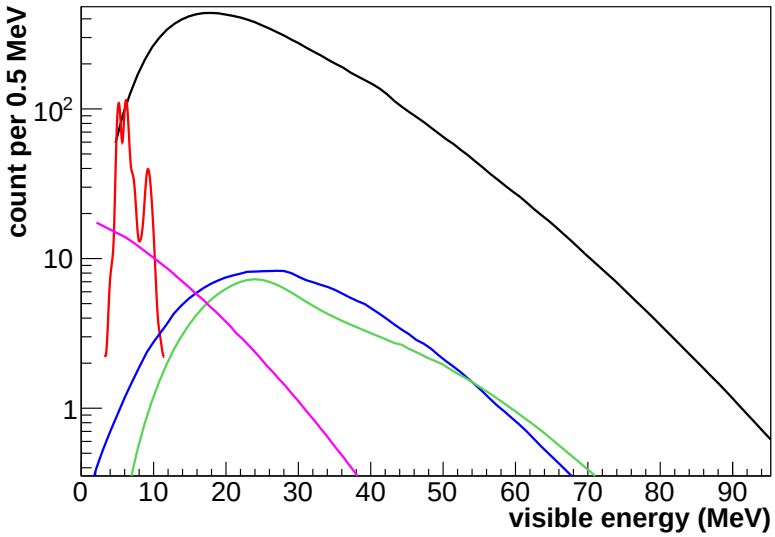

FIG. 9: Visible energy spectra for prompt events expected in 50 kt of WbLS, assuming a Gaussian energy resolution of 7 % at 1 MeV. Neutrino spectra and fluxes follow the GVKM model [**?**].

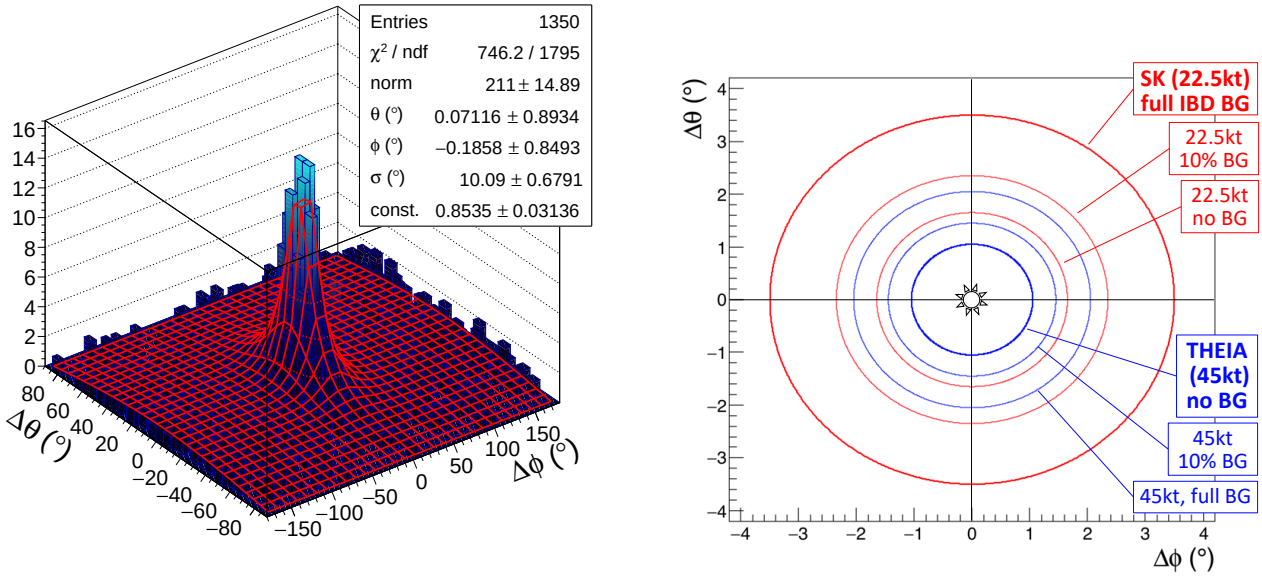

FIG. 10: SN pointing capability of THEIA, based on the reconstruction of the ES directional signal. *Left panel:* Example angular distribution, assuming 90 % in the flat IBD spectrum. Based on a fit to this and similar distributions (red net), the *right panel* depicts the pointing accuracy for THEIA, assuming different IBD background levels for 45 kt as well as 22.5 kt target mass.